Research Square

Preprints are preliminary reports that have not undergone peer review.
They should not be considered conclusive, used to inform clinical practice,
or referenced by the media as validated information.

Reproducible Coordinated P--Q Dispatch Optimization of a Smart-Inverter BESS for PV--EV Distribution Networks

Thananan Chooseang
Pathum Thani Technical College, Institute of Vocational Education Central Region 1
Siriwat Ninlawat
Nakhon Phanom University
Prakasit Prabpal
Udon Thani Technical College, Institute of Vocational Education Northeastern Region 1
Somchat Sonasang
Nakhon Phanom University
Niwat Angkawisittpan
Mahasarakham University
Praphat Phuangchuen
Institute of Vocational Education Eastern Region
Thunyaput Kittiphotiklang
thunyaput.k@technicrayong.ac.th

Institute of Vocational Education Eastern Region

Research Article

Keywords: battery energy storage system, smart inverter, active–reactive power dispatch, distribution network, electric vehicle charging, voltage regulation

Posted Date: October 30th, 2026

DOI: https://doi.org/10.21203/rs.3.rs-11317586/v1

License: This work is licensed under a Creative Commons Attribution 4.0 International License.
Read Full License

Additional Declarations: No competing interests reported.

Reproducible Coordinated P–Q Dispatch Optimization of a Smart-Inverter BESS for PV–EV Distribution Networks

Thananan Chooseang[1], Siriwat Ninlawat[2], Prakasit Prabpal[3], Somchat Sonasang[4], Niwat Angkawisittpan[5], Praphat Phuangchuen[6], Thunyaput Kittiphotiklang[7*]

[1]Department of Electronic Technology, Pathum Thani Technical College, Institute of Vocational Education Central Region 1, Pathum Thani, 12000, Thailand.
[2]Department of Electrical Technology, Faculty of Industrial Technology, Nakhon Phanom University, Nakhon Phanom, 48000, Thailand.
[3]Department of Electrical Technology, Udon Thani Technical College, Institute of Vocational Education Northeastern Region 1, Udon Thani, 41000, Thailand.
[4]Electrical Elements and Wireless Devices Unit (EEWDU), Faculty of Industrial Technology, Nakhon Phanom University, Nakhon Phanom, 48000, Thailand.
[5]Research Unit for Electrical and Computer Engineering Technology (RECENT), Faculty of Engineering, Mahasarakham University, Maha Sarakham, 44150, Thailand.
[6]Department of Mechanical Technology, Institute of Vocational Education Eastern Region, Rayong, 21000, Thailand.
[7*]Department of Electrical Technology, Institute of Vocational Education Eastern Region, Rayong, 21000, Thailand.

*Corresponding author(s). E-mail(s): thunyaput.k@technicrayong.ac.th;
Contributing authors: thananan@pttc.ac.th; siriwut.n@npu.ac.th; prakasit.pra@udontech.ac.th; somchat.s@npu.ac.th; niwat.a@msu.ac.th; praphat.p@technicrayong.ac.th;

Abstract

This study develops a 24-hour coordinated active- and reactive-power dispatch framework for a battery energy storage system (BESS) interfaced through a four-quadrant smart inverter in a radial distribution network with photovoltaic generation and electric-vehicle charging. The IEEE 33-bus feeder is evaluated under identical operating profiles and fixed hardware for three cases: no BESS, optimized active-power-only dispatch, and coordinated P–Q dispatch. A backward/forward-sweep power-flow solver is integrated with sequential least-squares programming to minimize a normalized objective combining feeder active-energy loss and system-wide voltage deviation, subject to BESS power limits, inverter apparent-power capability, charge/discharge efficiencies, state-of-charge (SOC) bounds, and terminal SOC equality. For an 800-kWh BESS with a 200-kW active-power limit and a 250-kVA inverter connected at Bus 18, P-only dispatch reduces daily feeder loss by 2.65%, whereas coordinated P–Q dispatch reduces it from 4267.86 to 3842.57 kWh/day, corresponding to a 9.97% reduction. The coordinated strategy further decreases daily voltage deviation by 17.77% and improves the worst-case minimum bus voltage from 0.83871 to 0.86695 p.u. The SOC remains within 19.41–95.00% and returns to 50% at the end of the scheduling horizon. Under deterministic load, PV, and EV perturbations applied without re-optimization, the fixed P–Q schedule maintains feeder-loss reductions of 9.42–10.61% and voltage-deviation reductions of 16.48–19.37%. These results demonstrate the additional network benefit of coordinated reactive-power support while also revealing the practical limitations imposed by fixed inverter capacity.

Keywords: battery energy storage system, smart inverter, active–reactive power dispatch, distribution network, electric vehicle charging, voltage regulation

1 Introduction

Distribution networks are increasingly affected by the combined variability of photovoltaic (PV) generation, electric-vehicle (EV) charging, and converter-interfaced distributed energy resources (DERs). Uncoordinated EV charging can increase feeder loading, active-power losses, and voltage deviations (Clement-Nyns et al. 2010; Richardson 2013), while increasing PV penetration introduces additional voltage-regulation requirements, particularly in radial distribution feeders (Turitsyn et al. 2011; Demirok et al. 2011; Dall'Anese et al. 2014a). Battery energy storage systems (BESSs) provide an additional degree of operational flexibility by shifting active power across time. When connected through a four-quadrant smart inverter, a BESS can also exchange reactive power with the network, allowing the available converter capacity to support both energy management and voltage regulation.

The capability of converter-interfaced DERs to provide active- and reactive-power support is increasingly recognized in modern interconnection and distribution-control practice. IEEE Std. 1547-2018 establishes interconnection and interoperability requirements for DERs, while IEEE Std. 1547.9-2022 provides additional guidance for energy-storage DERs capable of bidirectional active- and reactive-power exchange (IEEE

2018, 2022a). IEEE Std. 1885-2022 further addresses the assessment and verification of distribution Volt/VAR control and optimization (IEEE 2022b). These developments reflect the broader transition from fixed or unity-power-factor converter operation toward multifunctional smart inverters capable of providing voltage and ancillary support (Mirafzal and Adib 2020).

A substantial body of research has examined the use of inverter reactive-power capability in distribution networks. Centralized, local, sensitivity-based, and droop-based strategies have demonstrated that reactive-power control can improve voltage profiles and, under suitable operating conditions, reduce feeder losses (Turitsyn et al. 2011; Demirok et al. 2011; Farivar et al. 2012). Optimization-based approaches have further considered coordinated active- and reactive-power dispatch, decentralized implementation, and uncertainty-aware operation (Dall'Anese et al. 2014a,b, 2015; Singhal et al. 2019). More recent studies have extended these concepts to coordinated Volt/VAR devices, multiperiod DER scheduling, and BESS-assisted voltage support (Long and Kirschen 2022; Gebbran et al. 2023; Hu et al. 2022).

The inclusion of energy storage introduces an important temporal dimension that distinguishes BESS dispatch from instantaneous inverter Volt/VAR control. BESS operation is constrained not only by converter power limits but also by energy capacity, charging and discharging efficiencies, state-of-charge (SOC) limits, and intertemporal energy balance. Previous studies have therefore examined BESS placement and sizing, coordinated PV/BESS operation, hosting-capacity improvement, and simultaneous active- and reactive-power support (Wong et al. 2019; Das et al. 2018; Yuan et al. 2020; Ahlawat and Das 2023; Khajeh et al. 2023; Gush et al. 2021; Ghazavi Dozein et al. 2021). In parallel, EV-oriented studies have quantified the adverse effects of concentrated charging and investigated the use of converter-based EV resources for voltage and reactive-power support (Soofi and Manshadi 2023; Wu and Liu 2023). Together, these studies establish the technical value of coordinated converter control, but they also show that the achievable benefit depends strongly on device rating, electrical location, network condition, and available inverter headroom.

Table 1 summarizes the main research streams relevant to the present study and clarifies its position relative to existing work. Rather than proposing a new global optimization paradigm or a new BESS-sizing method, this study focuses on a narrower operational question: *for fixed BESS hardware, a fixed smart-inverter rating, and an identical 24-hour PV–EV–load scenario, how much additional network benefit is obtained when reactive-power capability is coordinated with active-power dispatch?* This controlled comparison is intended to separate the contribution of inverter VAR capability from improvements that could otherwise arise from changes in storage size, converter rating, placement, or external operating profiles.

Two methodological considerations are particularly important in interpreting such a comparison. First, the term "optimal" should refer only to the variables actually optimized; the fixed BESS energy capacity, converter rating, and installation location used here are therefore treated as prescribed hardware rather than as optimally sized design variables. Second, improved voltage performance should be distinguished from voltage compliance. If the available inverter capacity is insufficient to maintain all bus voltages within a reference band, the result should be reported as voltage-profile

mitigation rather than complete voltage restoration. These distinctions are retained throughout the present study to avoid overstating the capability of the proposed dispatch strategy.

Accordingly, this work develops a reproducible 24-hour comparison of three operating cases: a PV–EV base case without BESS support, an optimized active-power-only BESS schedule, and coordinated active–reactive power dispatch using the same storage and inverter hardware. The study makes four main contributions. First, the IEEE 33-bus feeder is implemented using a backward/forward-sweep power-flow solver and verified against a nominal-load benchmark before the time-series analysis. Second, a constrained sequential least-squares programming formulation coordinates hourly BESS active and reactive power while enforcing the inverter apparent-power capability, SOC bounds, charge/discharge efficiencies, and terminal SOC equality. Third, the controlled P-only/P–Q comparison isolates the incremental contribution of reactive-power capability under identical network, hardware, PV, EV, and load conditions. Fourth, an open-loop perturbation assessment applies the nominal optimized P–Q schedule without re-optimization to changes in feeder loading, PV generation, and EV demand, thereby distinguishing persistence of the mitigation benefit from guaranteed voltage compliance. All reported numerical results and figures are generated from the same implemented power-flow and dispatch model to maintain internal consistency and reproducibility.

2 Related Work and Research Gap

Existing research provides strong foundations for both distribution-network analysis and inverter-assisted voltage control. Radial load-flow methods based on backward/forward sweeps and related direct formulations are well established for distribution systems because they exploit radial topology and efficiently accommodate nonlinear constant-power loads (Teng 2003; Eminoglu and Hocaoglu 2009). These methods provide an appropriate inner network solver for multiperiod optimization in which feeder voltages and losses must be repeatedly evaluated for different DER operating points.

A closely related research stream concerns the active- and reactive-power capabilities of smart inverters. Reactive-power control of converter-interfaced DERs has been shown to improve distribution-network voltage profiles and, depending on network conditions and the control objective, reduce feeder losses (Turitsyn et al. 2011; Demirok et al. 2011; Farivar et al. 2012). Optimization-based formulations have subsequently incorporated coordinated active and reactive power, decentralized control, uncertainty, adaptive Volt/VAR behavior, and interactions with conventional voltage-regulation equipment (Dall'Anese et al. 2014a,b, 2015; Singhal et al. 2019; Yoshizawa et al. 2021; Long and Kirschen 2022). Related studies have also considered hosting-capacity enhancement and distributed Volt/VAR or Volt/Watt control (Ustun et al. 2019; Babu and Khatod 2024). Collectively, this literature establishes the effectiveness of inverter VAR capability but focuses predominantly on PV inverters, multiple DERs, voltage-control architectures, or broader optimal-power-flow formulations.

The presence of a BESS introduces intertemporal energy constraints that are absent from instantaneous inverter Volt/VAR control. Multiperiod DER optimization has therefore incorporated BESS operation, coordinated active/reactive dispatch, and PV–storage interaction (Gebbran et al. 2023; Hu et al. 2022; Gush et al. 2021). At the same time, EV charging introduces an additional time-varying feeder stress. Earlier studies demonstrated that uncontrolled EV charging can increase distribution losses and aggravate voltage deviations (Clement-Nyns et al. 2010), while more recent formulations have considered EV and PV converters themselves as reactive-power resources (Soofi and Manshadi 2023). These studies demonstrate the importance of temporal coordination but generally address broader resource coordination, planning, or converter-control problems.

The specific gap considered in this work is therefore narrower. As summarized in Table 1, comparatively limited attention has been given to a controlled comparison in which the BESS energy capacity, active-power rating, inverter apparent-power rating, installation bus, and external PV–EV–load profiles are all held fixed while only the available inverter control degrees of freedom are changed. Without such a controlled comparison, the incremental contribution of reactive-power capability can be difficult to distinguish from benefits associated with storage sizing, converter oversizing, placement, or different operating scenarios.

Accordingly, the present study compares active-power-only and coordinated P–Q BESS dispatch under identical fixed hardware and identical 24-hour operating profiles while enforcing storage-energy neutrality through a terminal-SOC constraint. The analysis additionally retains residual undervoltage rather than interpreting voltage improvement as voltage compliance and evaluates the nominal coordinated schedule under deterministic load, PV, and EV perturbations without re-optimization. The resulting formulation is intended to quantify the incremental network value—and the practical limitation—of smart-inverter reactive-power capability for a fixed BESS installation, rather than to claim globally optimal BESS sizing, placement, or feeder-wide voltage restoration.

3 System Model and Optimization Framework

Figure 1 summarizes the 24-hour coordinated active–reactive power dispatch framework considered in this study. Hourly feeder loading, PV generation, and EV charging profiles are supplied to a constrained SLSQP optimizer, within which a backward/forward-sweep (BFS) power-flow solver evaluates the network state for each candidate BESS dispatch schedule. The BESS is connected at Bus 18 through a 250-kVA four-quadrant smart inverter. Performance is evaluated in terms of daily feeder active-energy loss, bus-voltage behavior, voltage-deviation index (VDI), and BESS state of charge (SOC).

3.1 IEEE 33-Bus Radial Distribution System

The network model is based on the Baran–Wu 33-bus radial distribution system implemented from the MATPOWER `case33bw` data set (Baran and Wu 1989; Zimmerman et al. 2011). The nominal line-to-line voltage is 12.66 kV, and the total base load

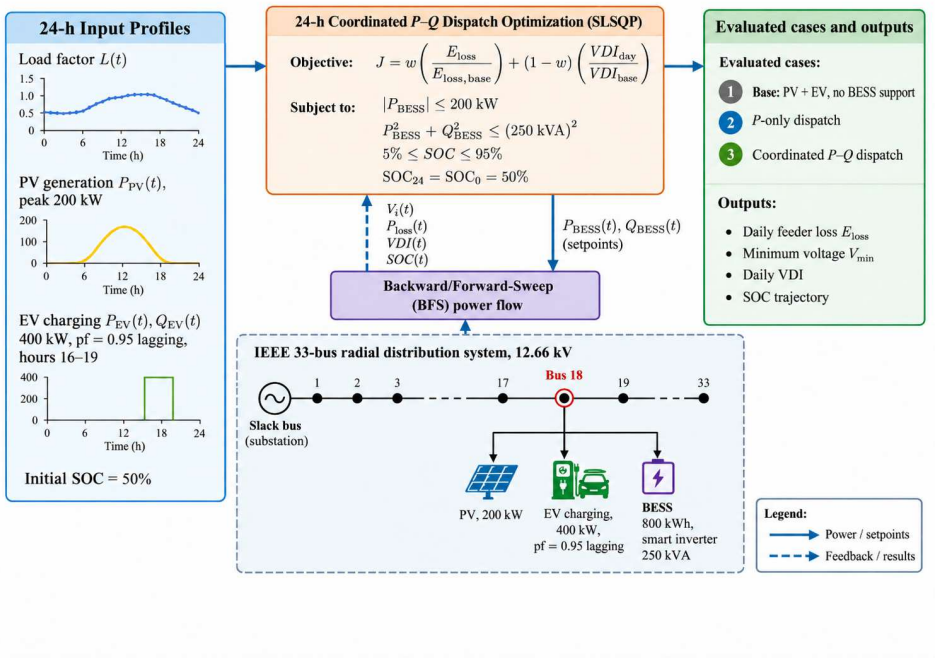


Fig. 1 Twenty-four-hour coordinated P–Q dispatch framework for the smart-inverter BESS connected at Bus 18 of the IEEE 33-bus radial distribution system.

is 3.715 MW and 2.300 MVAr. Before applying the 24-hour operating profiles, the implemented BFS solver was evaluated at nominal loading without PV, EV, or BESS injections. The resulting feeder active-power loss was 202.677 kW, with a minimum bus voltage of 0.91309 p.u. at Bus 18. This benchmark calculation was used to verify the implemented feeder data and power-flow solution before optimization.

For each hour t, the net complex power at bus i is represented as

$$S_i(t) = L(t)\,(P_{i,0} + jQ_{i,0}) + S_{i,\mathrm{EV}}(t) - S_{i,\mathrm{PV}}(t) - S_{i,\mathrm{BESS}}(t), \tag{1}$$

where $P_{i,0}$ and $Q_{i,0}$ are the nominal active and reactive loads, respectively, and $L(t)$ is the hourly feeder-load factor. In the present configuration, the PV source, EV charging demand, and BESS are all connected at Bus 18.

At BFS iteration k, the bus injection current is calculated as

$$I_i^{(k)}(t) = \left(\frac{S_i(t)}{V_i^{(k)}(t)}\right)^*, \tag{2}$$

where $(\cdot)^*$ denotes the complex conjugate. Branch currents are accumulated from the terminal buses toward the slack bus during the backward sweep. Bus voltages are then

updated in the forward sweep according to

$$V_j^{(k+1)}(t) = V_i^{(k+1)}(t) - Z_{ij} I_{ij}^{(k)}(t), \tag{3}$$

where Z_{ij} is the impedance of the branch connecting buses i and j. Iteration continues until the maximum change in complex bus voltage between successive iterations is below 10^{-9} p.u.

The active-power loss at hour t is calculated from

$$P_{\text{loss}}(t) = 1000 S_{\text{base}} \sum_{\ell=1}^{32} R_{\ell,\text{pu}} \left| I_\ell(t) \right|^2 \quad [\text{kW}], \tag{4}$$

where S_{base} is expressed in MVA, so the factor 1000 converts the calculated loss from MW to kW. The corresponding daily active-energy loss is

$$E_{\text{loss}} = \sum_{t=1}^{24} P_{\text{loss}}(t) \Delta t, \qquad \Delta t = 1 \text{ h}. \tag{5}$$

3.2 PV, EV, and Daily Loading Scenario

Figure 2 shows the deterministic 24-hour profiles used in the study. The PV source at Bus 18 has a peak active-power output of 200 kW. The EV charging hub introduces an additional 400 kW during hours 16–19 at a lagging power factor of 0.95, corresponding to approximately 131.47 kVAr of reactive demand during the charging interval. The nominal feeder loads are scaled using the hourly load factor shown in the same figure.

These profiles are intentionally treated as prescribed operating trajectories rather than probabilistic forecasts. This construction permits the three operating cases to be compared under identical external conditions so that differences between P-only and coordinated P–Q operation can be attributed to the available inverter-control degrees of freedom rather than to changes in the underlying load, PV, or EV profiles.

3.3 BESS and Smart-Inverter Constraints

The fixed storage system consists of an 800-kWh BESS with an active-power limit of ± 200 kW connected through a 250-kVA four-quadrant smart inverter. The initial SOC is 50%, the allowable operating range is 5–95%, and both charging and discharging efficiencies are 95%. Positive P_{BESS} denotes discharge from the BESS to the feeder, whereas negative P_{BESS} denotes charging.

The SOC transition is modeled as

$$\text{SOC}_t = \text{SOC}_{t-1} - \begin{cases} \dfrac{P_t \Delta t}{\eta_d E_{\text{BESS}}}, & P_t \geq 0, \\ \dfrac{\eta_c P_t \Delta t}{E_{\text{BESS}}}, & P_t < 0, \end{cases} \qquad t = 1, \ldots, 24. \tag{6}$$

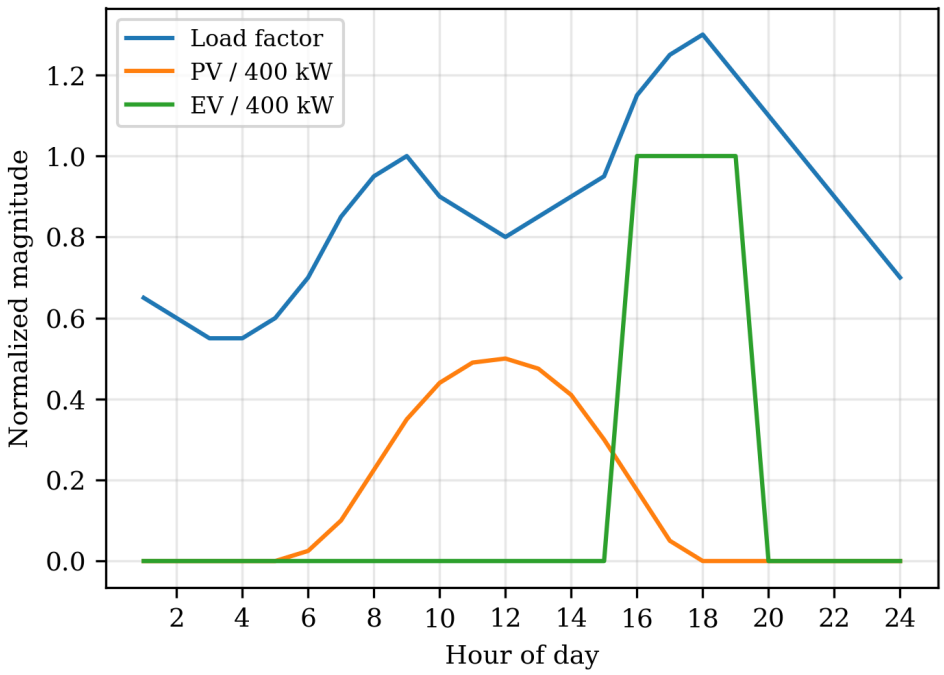


Fig. 2 Hourly feeder-load, PV-generation, and EV-charging profiles used in the 24-hour study. The PV source has a 200-kW peak output, while EV charging reaches 400 kW during hours 16–19.

where E_{BESS} is the rated storage capacity, and η_c and η_d are the charging and discharging efficiencies, respectively. The corresponding operating constraints are

$$-200 \le P_t \le 200 \text{ kW}, \tag{7}$$

$$0.05 \le \mathrm{SOC}_t \le 0.95, \tag{8}$$

$$\mathrm{SOC}_{24} = \mathrm{SOC}_0 = 0.50. \tag{9}$$

The terminal-SOC equality enforces daily energy neutrality at the storage level and prevents an artificially favorable solution obtained by ending the scheduling horizon with a depleted battery.

For coordinated P–Q operation, active and reactive powers share the same inverter apparent-power capacity:

$$P_t^2 + Q_t^2 \le S_{\mathrm{inv}}^2, \qquad S_{\mathrm{inv}} = 250 \text{ kVA}. \tag{10}$$

Thus, increased active-power exchange reduces the reactive-power capability available at the same operating point, and vice versa. In the P-only comparison, Q_t is fixed at zero while the BESS energy capacity, active-power limits, efficiencies, SOC constraints, and terminal-SOC requirement remain unchanged.

3.4 Voltage-Deviation Metric and Optimization Objective

To characterize feeder-wide voltage behavior rather than relying solely on the minimum bus voltage, the hourly voltage-deviation index is defined as

$$\mathrm{VDI}(t) = \sum_{i=1}^{33} \left(|V_i(t)| - 1\right)^2 . \tag{11}$$

The corresponding daily index is

$$\mathrm{VDI}_{\mathrm{day}} = \sum_{t=1}^{24} \mathrm{VDI}(t). \tag{12}$$

Feeder energy loss and voltage deviation have different physical units and numerical magnitudes. They are therefore normalized by their corresponding values in the PV+EV base case before being combined into the scalar objective

$$J = w \frac{E_{\mathrm{loss}}}{E_{\mathrm{loss,base}}} + (1 - w) \frac{\mathrm{VDI}_{\mathrm{day}}}{\mathrm{VDI}_{\mathrm{base}}}, \tag{13}$$

where $w = 0.5$ is used for the principal comparison. Equal weighting is applied to the two normalized performance indices; it does not represent an economic equivalence between feeder energy loss and voltage deviation.

The constrained optimization problem is solved using sequential least-squares programming (SLSQP), which accommodates bound constraints, equality constraints, and nonlinear inequalities (Kraft 1988; Virtanen et al. 2020). The P-only formulation contains 24 hourly active-power variables,

$$[P_1, \ldots, P_{24}],$$

whereas the coordinated formulation contains 48 decision variables,

$$[P_1, \ldots, P_{24}, Q_1, \ldots, Q_{24}].$$

A deterministic zero vector is used as the initial point for reproducibility.

Because the optimization contains an embedded nonlinear AC distribution power-flow calculation, the resulting problem is nonconvex. SLSQP is therefore used as a local constrained optimizer, and the resulting schedule is interpreted as a locally optimized feasible solution rather than as a certified global optimum. This qualification is retained throughout the analysis.

A voltage magnitude of 0.95 p.u. is used as an engineering reference when presenting the results, but it is not imposed as a hard optimization constraint. For the fixed 250-kVA inverter and the specified severe loading and EV-charging scenario, the available converter capability does not eliminate all undervoltage conditions. Accordingly, the study evaluates the degree of voltage-profile mitigation achieved by coordinated P–Q dispatch and does not claim guaranteed feeder-wide voltage compliance.

4 Simulation Procedure and Reproducibility

The numerical implementation follows the high-level architecture in Fig. 1 and the detailed computational workflow in Fig. 3. While Section 3 defines the network, BESS, inverter, and optimization models, the present section describes how these models are assembled and executed to produce the reported results. The complete workflow is deterministic: the same network data, operating profiles, initial conditions, optimization formulation, and power-flow routine are used throughout the comparative and robustness analyses.

4.1 Computational Implementation

The simulation model was implemented in Python using NumPy and pandas for numerical and tabular data handling, SciPy for constrained optimization, and Matplotlib for generation of the reported figures. As summarized in Fig. 3, the workflow begins by defining the output directory used to store numerical results and publication figures. The IEEE 33-bus feeder data are then initialized, including the active- and reactive-power demands at each bus, branch resistance and reactance data, the nominal line-to-line voltage of 12.66 kV, and a system base of 10 MVA.

Because the feeder topology remains unchanged over the complete 24-hour analysis, topology-dependent quantities are precomputed before the optimization begins. These quantities include the parent–branch mapping, the downstream path information, and the branch-incidence structure used by the backward/forward-sweep (BFS) power-flow routine. Precomputing these network relationships avoids reconstructing the radial topology during every objective-function evaluation.

The prescribed 24-hour operating scenario is then loaded. It consists of the feeder load factor $L(t)$, the 200-kW peak PV-generation profile, and the EV charging profile with a 400-kW demand during hours 16–19 at a lagging power factor of 0.95. The BESS and smart-inverter parameters are subsequently initialized using the fixed hardware values defined in Section 3: an 800-kWh energy capacity, a $\pm$200-kW active-power limit, a 250-kVA inverter rating, an initial SOC of 50%, an SOC operating range of 5–95%, and charging and discharging efficiencies of 95%.

Three principal computational functions are then used throughout the analysis. The power-flow function evaluates all 24 hourly operating points using the BFS algorithm; the SOC function computes the BESS energy trajectory from a candidate active-power schedule; and the evaluation function combines the resulting feeder losses, voltage quantities, VDI, SOC states, and optimization constraints. The same functions are used during optimization and during final performance evaluation so that no separate approximation or post-processing model is introduced.

4.2 Power-Flow Verification and Operating Cases

Before the optimization is executed, the implemented IEEE 33-bus model is subjected to a static benchmark check, corresponding to Step 7 in Fig. 3. The feeder is evaluated at nominal load without PV generation, EV charging, or BESS support. As reported in Section 3, this calculation gives a feeder active-power loss of 202.677 kW and a minimum voltage of 0.91309 p.u. at Bus 18. This independent preliminary calculation

is used to verify the feeder data and BFS implementation before introducing time-varying resources or optimization variables.

The time-series study subsequently evaluates three operating cases under identical network data and identical external load, PV, and EV profiles:

1. *Base case*: PV generation and EV charging are applied at Bus 18, with no BESS support.
2. *Optimized P-only case*: the hourly BESS active-power schedule $P_{\mathrm{BESS}}(t)$ is optimized while $Q_{\mathrm{BESS}}(t) = 0$.
3. *Coordinated P–Q case*: both $P_{\mathrm{BESS}}(t)$ and $Q_{\mathrm{BESS}}(t)$ are optimized simultaneously while satisfying the BESS energy constraints and the 250-kVA inverter apparent-power capability.

The BESS energy capacity, active-power rating, inverter rating, installation bus, initial SOC, and all external operating profiles are held fixed between the P-only and P–Q cases. Consequently, their performance difference provides a controlled measure of the additional network benefit obtained from the inverter reactive-power degree of freedom.

4.3 BFS–SLSQP Computational Sequence

For each optimized operating case, the SLSQP procedure begins from the prescribed deterministic initial decision vector. At every objective- function evaluation, the candidate hourly setpoints are passed to the BESS and network models. The corresponding SOC trajectory is calculated, after which the BFS power-flow routine is executed for each of the 24 one-hour intervals.

Within each hourly BFS calculation, bus injection currents are first computed from the current bus voltages and specified complex powers. Branch currents are then accumulated from downstream buses toward the slack bus, followed by a forward sweep that updates the bus voltages from the slack bus toward the feeder terminals. These backward and forward sweeps are repeated until the maximum complex-voltage change satisfies the convergence tolerance of 10^{-9} p.u. A maximum of 100 BFS iterations is imposed for each hourly power-flow solution.

Once all 24 hourly power-flow calculations have been completed, the evaluation routine returns the bus-voltage magnitudes, hourly feeder losses, VDI values, and BESS SOC states to the optimization routine. The daily active-energy loss and daily VDI are then formed and used in the normalized objective function defined in Eq. (13). The active-power bounds, SOC limits, terminal-SOC equality, and inverter apparent-power constraint are checked for the candidate schedule. SLSQP subsequently updates the decision variables and repeats this process until its convergence condition is satisfied.

For the P-only case, the decision vector contains the 24 hourly values of $P_{\mathrm{BESS}}(t)$. For the coordinated case, the decision vector contains 48 variables corresponding to $P_{\mathrm{BESS}}(t)$ and $Q_{\mathrm{BESS}}(t)$ over the complete 24-hour horizon. The optimized setpoints are retained only after the complete network and storage constraints have been evaluated through the same BFS–SOC calculation chain.

4.4 Performance Evaluation and Data Generation

Following optimization, each operating case is evaluated again using the same power-flow implementation to obtain the final performance indices. The principal quantities retained for comparison are

- daily feeder active-energy loss E_{loss},
- daily voltage-deviation index VDI_{day},
- minimum bus voltage V_{min} over the 24-hour horizon,
- number of bus-hour voltage points below the 0.95-p.u. engineering reference, and
- BESS SOC trajectory.

The 0.95-p.u. level is used only as a reporting reference. It is not included as a hard optimization constraint because the fixed 250-kVA inverter at Bus 18 is unable to maintain every bus above this level under the specified severe loading and EV-charging conditions. The analysis therefore distinguishes improvement of the voltage profile from feeder-wide voltage compliance.

The computed hourly and aggregate results are exported directly from the implemented model and are subsequently used to generate the loss, voltage, P–Q dispatch, SOC, VDI, and aggregate-performance figures. Because these figures and tables are produced from the same numerical data used in the optimization, the graphical and tabulated results remain internally consistent with the reported dispatch solution.

After the nominal cases have been completed, the final coordinated P–Q schedule is also subjected to the open-loop robustness tests shown in the last stage of Fig. 3. These tests include ±10% feeder-load variation, ±20% PV-generation variation, ±20% EV-demand variation, and combined favorable and stress conditions. Importantly, the nominal P–Q schedule is kept fixed and is *not re-optimized* for the perturbed scenarios. The robustness analysis therefore evaluates persistence of the mitigation benefit under profile mismatch rather than the performance of an adaptive or scenario-specific controller.

Table 2 summarizes the principal network, resource, storage, and numerical parameters used throughout the simulation.

Figure 3 summarizes the complete implemented sequence. The workflow proceeds from network and scenario initialization, through static feeder validation and case selection, to the nested BFS–SLSQP optimization. The resulting 24-hour performance indices are then exported and used to generate the publication figures, compare the three principal operating cases, and perform the final open-loop robustness assessment.

5 Results and Discussion

The results are evaluated from both network- and converter-level perspectives. The prescribed 24-hour load, PV-generation, and EV-charging profiles are applied identically to the base, optimized P-only, and coordinated P–Q cases. Consequently, differences between the two optimized cases can be interpreted primarily in terms of the additional reactive-power capability of the smart inverter rather than differences in BESS size, converter rating, installation location, or external operating conditions. The discussion first examines feeder energy loss and voltage performance, then relates

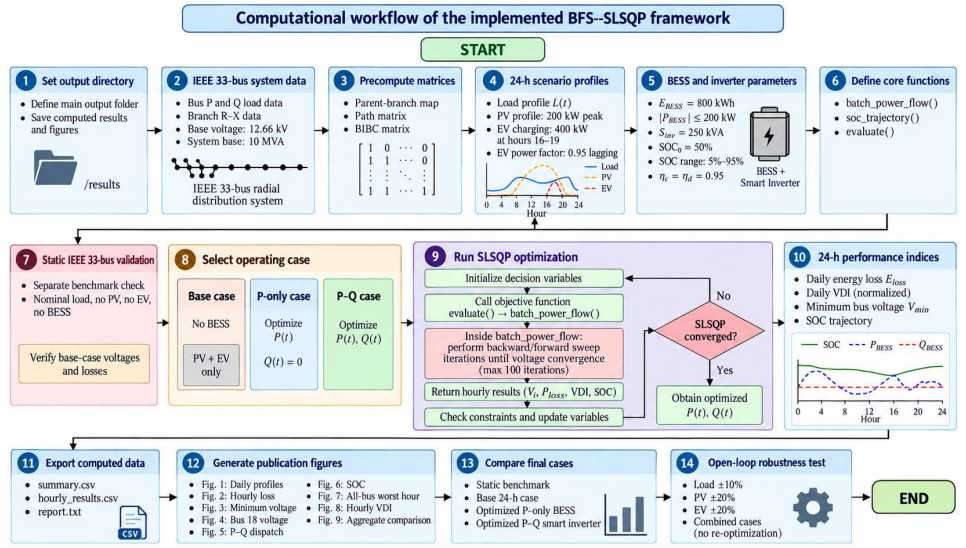


Fig. 3 Detailed computational workflow of the implemented BFS–SLSQP framework, including data initialization, static feeder validation, operating-case selection, constrained 24-hour optimization, performance evaluation, data export, figure generation, case comparison, and open-loop robustness testing without re-optimization.

these network responses to the optimized BESS dispatch and inverter capability, and finally evaluates sensitivity to profile perturbations and numerical solver behavior.

5.1 Twenty-Four-Hour Feeder Performance

Table 3 summarizes the principal network-performance indices over the complete 24-hour operating horizon. In the base case, which includes PV generation and EV charging but no BESS support, the feeder active-energy loss is 4267.862 kWh/day. Optimizing only the BESS active-power trajectory reduces the loss to 4154.861 kWh/day, corresponding to a 2.648% reduction. When the reactive-power degree of freedom is included, the coordinated P–Q dispatch reduces the daily loss further to 3842.568 kWh/day, or 9.965% below the base case.

The comparison between the P-only and P–Q cases is particularly important because both employ the same 800-kWh BESS, ±200-kW active-power limit, 250-kVA inverter, connection bus, and operating profiles. The coordinated case reduces daily feeder loss by an additional 312.293 kWh/day relative to the P-only schedule, equivalent to approximately 7.52% of the P-only loss. From an electrical-network perspective, active-power discharge reduces the real-power transfer through the upstream feeder branches, whereas local reactive-power injection reduces the reactive-power component that would otherwise be supplied from the substation. Both effects decrease branch-current magnitude and therefore reduce resistive I^2R losses.

A similar improvement is observed in the feeder-wide voltage-deviation index. The daily VDI decreases from 2.511772 in the base case to 2.434206 with P-only dispatch and to 2.065514 with coordinated P–Q dispatch. The corresponding reductions are

3.088% and 17.767%, respectively. Relative to P-only operation, coordinated dispatch provides a further 15.15% reduction in daily VDI. The substantially larger improvement in VDI than in the P-only case indicates that reactive-power control provides a direct voltage-support mechanism in addition to the voltage improvement obtained indirectly through active-power reduction of feeder loading.

Figure 4 shows the hourly active-power losses. The temporal variation follows the load, PV, and EV profiles shown in Fig. 2. The most severe condition occurs at hour 18, when feeder loading is high and the 400-kW EV charging demand is active. At this hour, the feeder loss is 485.918 kW in the base case, 425.992 kW with P-only dispatch, and 411.638 kW with coordinated P–Q dispatch. Thus, the coordinated strategy lowers the hour-18 loss by approximately 15.29% relative to the base system.

This reduction can be interpreted directly from radial-feeder power flow. During a high-load interval, supplying part of the local active demand from the BESS reduces upstream active-power flow. Simultaneously, capacitive reactive-power injection reduces the reactive current supplied through the feeder. Because branch losses depend on the square of current magnitude, coordinating these two mechanisms is more effective than manipulating active power alone.

The benefit is not uniform over all hours. When the BESS is charging, it appears to the feeder as an additional active-power demand. Some energy discharged during high-stress periods must therefore be recovered during other intervals to satisfy the terminal-SOC equality. For this reason, daily active-energy loss is a more meaningful performance measure than the loss at an individual hour. The 9.965% daily reduction is achieved while returning the BESS to its initial SOC and therefore cannot be attributed to net depletion of stored energy.

The voltage response exhibits the same electrical loading dependence. Figure 5 presents the minimum bus voltage at each hour. The lowest voltage occurs at hour 18, coincident with the high-load and EV-charging condition. The worst minimum voltage is 0.83871 p.u. in the base case, increases to 0.85732 p.u. with P-only dispatch, and reaches 0.86695 p.u. with coordinated P–Q dispatch. The absolute improvement provided by coordinated operation is therefore 0.02824 p.u. relative to the base system.

Reactive-power injection is particularly effective in this radial feeder because it reduces the reactive-power transfer through electrically remote branches and consequently reduces the associated voltage drop. Nevertheless, the minimum voltage remains below the 0.95-p.u. engineering reference. The result should therefore be interpreted as mitigation of undervoltage, not restoration of the complete feeder to an acceptable voltage band.

The number of bus-hour voltage points below 0.95 p.u. provides a broader view of the time-dependent voltage condition. Coordinated P–Q operation reduces this count from 338 in the base case to 282. In contrast, the P-only case produces 355 bus-hour points below the reference even though its absolute worst-case voltage improves. This apparently contradictory behavior is a consequence of intertemporal energy balancing. Active power discharged during highly stressed intervals must later be replenished, and BESS charging can increase feeder demand during other hours. Thus, a single minimum-voltage value cannot by itself describe the complete 24-hour voltage performance.

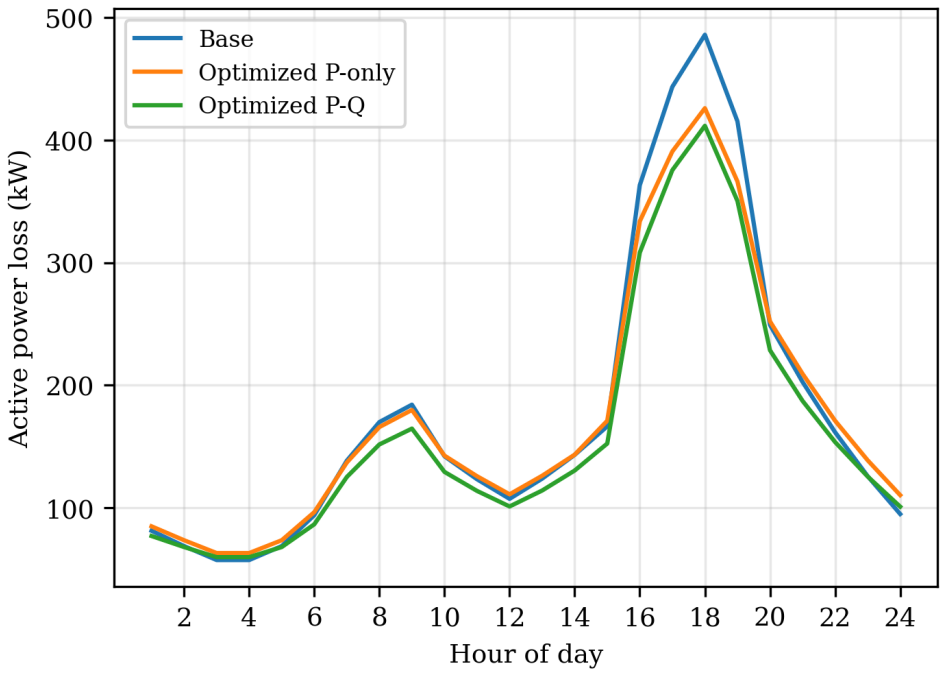


Fig. 4 Hourly active-power loss for the base, optimized P-only, and coordinated P–Q operating cases.

This behavior is further reflected in the hourly VDI shown in Fig. 6. Unlike the minimum-voltage metric, which represents only one bus at one instant, the VDI measures the aggregate displacement of all 33 bus voltages from 1.0 p.u. Coordinated P–Q operation produces the lowest VDI over most of the daily horizon, with the greatest improvement occurring during electrically stressed periods.

The normalized daily comparison in Fig. 7 reinforces this observation. P-only scheduling produces relatively modest reductions in both indices, whereas coordinated P–Q operation substantially improves feeder energy loss and system-wide voltage deviation. Reactive-power support does not require direct exchange of electrochemical energy, but it is not unconstrained: the required VAR output occupies part of the same inverter apparent-power capacity used for active-power exchange.

5.2 Smart-Inverter Dispatch, SOC, and Spatial Voltage Response

The local voltage at Bus 18 is of particular interest because the PV source, EV charging demand, and BESS are all connected at this bus. Figure 8 shows that P-only control improves the Bus 18 voltage primarily by reducing local net active-power demand during high-stress periods. Coordinated P–Q control provides an additional voltage-support mechanism through reactive-power injection. The improvement is most pronounced during the evening interval in which feeder loading and EV charging occur simultaneously.

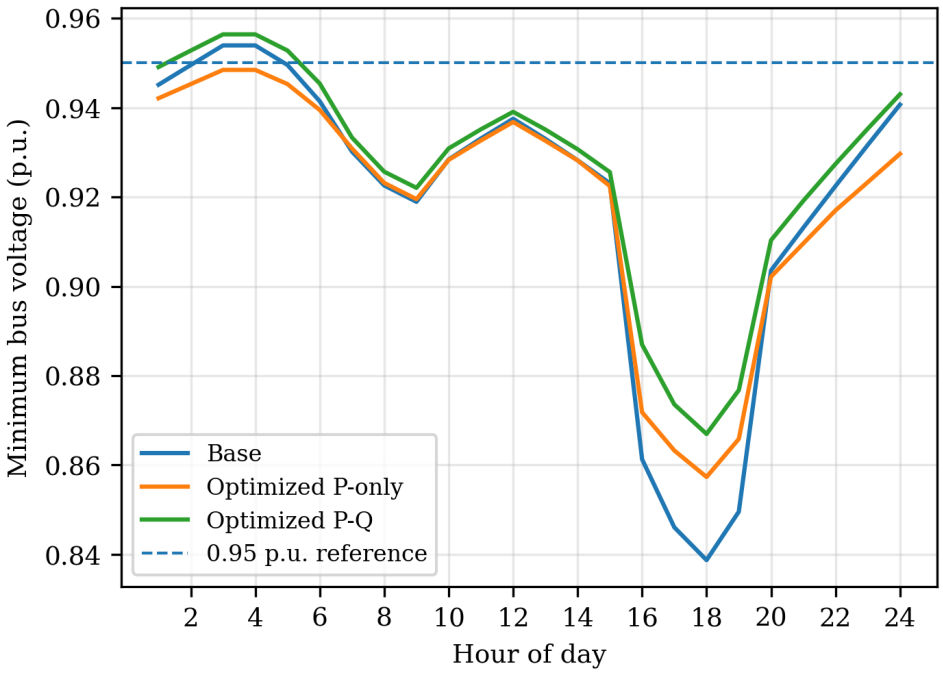


Fig. 5 Minimum bus voltage over the 24-hour simulation. The 0.95-p.u. line is shown as an engineering reference and is not imposed as a hard voltage constraint.

Local voltage improvement does not imply that the complete radial feeder satisfies the voltage reference. Figure 9 therefore presents the spatial voltage profile of all 33 buses at the base-case worst operating hour. Coordinated P–Q dispatch raises the voltage along the electrically remote portion of the feeder, including the section containing Bus 18. However, several buses remain below 0.95 p.u., demonstrating that the available reactive-power support is limited by both inverter rating and electrical location.

The optimized converter operating trajectory shown in Fig. 10 provides the device-level explanation for these network results. The active power varies from approximately -132.16 to $+152.90$ kW, remaining within the specified ± 200-kW BESS power limit. Positive active power corresponds to discharge into the feeder, whereas negative power represents battery charging.

The optimized reactive-power output remains capacitive over the reported solution and ranges from approximately 197.79 to 250 kVAr. Such operation is consistent with the voltage-depressed feeder condition because local reactive-power injection reduces the VAR demand supplied through upstream branches and increases the voltage at electrically remote buses.

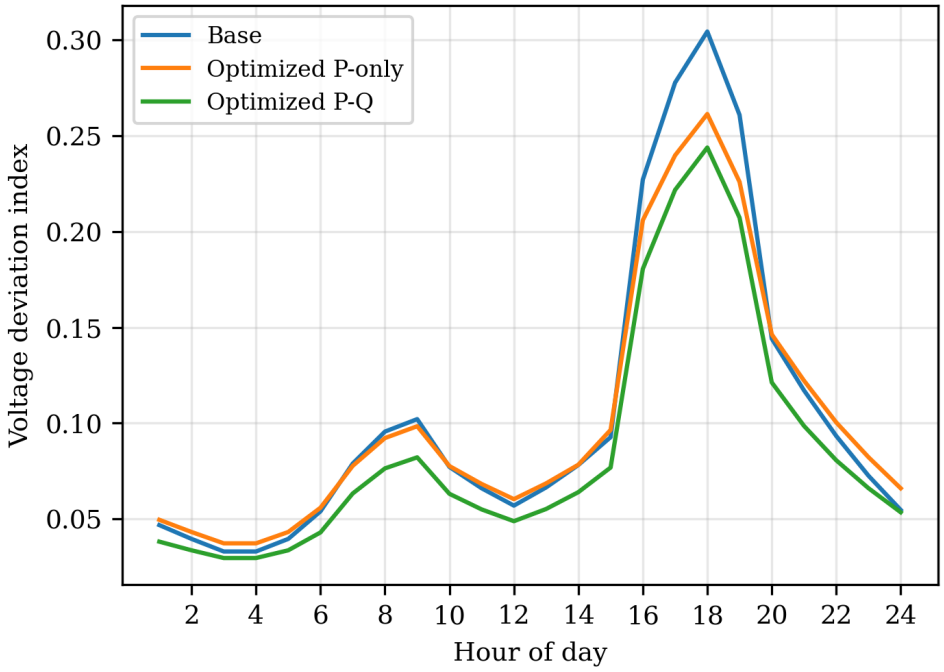


Fig. 6 Hourly voltage-deviation index for the base, optimized P-only, and coordinated P–Q cases.

The important engineering constraint is that active and reactive powers are not independently available. They must satisfy

$$P_{\mathrm{BESS}}^2 + Q_{\mathrm{BESS}}^2 \leq S_{\mathrm{inv}}^2,$$

with $S_{\mathrm{inv}} = 250$ kVA. Therefore, increasing the magnitude of active-power exchange reduces the available reactive-power headroom. Conversely, operating close to the maximum VAR output limits the active power that can be delivered simultaneously. The optimized trajectory should thus be interpreted as allocation of a finite converter kVA capability between active-energy transfer and voltage support.

Figure 11 shows the corresponding battery-energy trajectory. The SOC remains between 19.41% and 95.00%, within the prescribed 5–95% operating range, and returns to 50% at the end of the 24-hour horizon. The terminal-SOC requirement is essential for a fair comparison because otherwise the optimizer could improve feeder performance by extracting net battery energy during the study period and leaving the recharging requirement outside the modeled horizon.

The coordinated result therefore represents redistribution of BESS active energy over time together with reactive-power support from the inverter, rather than one-way depletion of the storage system. This distinction is important when interpreting the reported daily loss reduction as an operational network benefit.

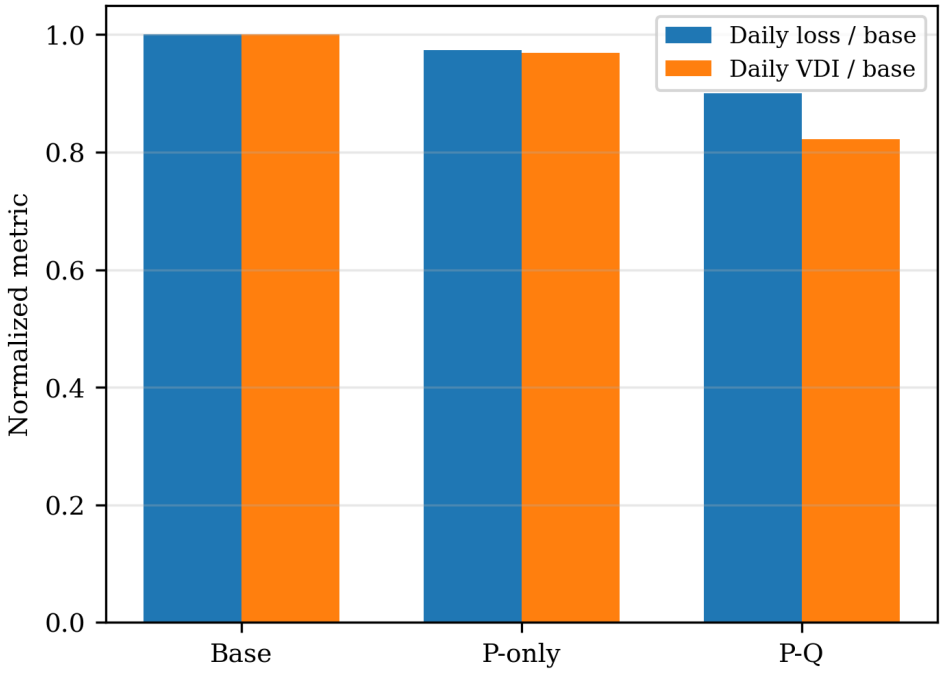


Fig. 7 Normalized daily active-energy loss and daily voltage-deviation index. Each metric is normalized by its corresponding base-case value.

5.3 Robustness and Numerical Behavior

The nominal coordinated schedule was subsequently applied to perturbed operating profiles without re-optimization. This open-loop test is intended to examine whether the network benefit obtained from the nominal schedule persists when the actual operating condition differs from that assumed during optimization. It should therefore be distinguished from stochastic, adaptive, or scenario-specific re-optimization.

The perturbations include ±10% feeder-load variation, ±20% PV-generation variation, and ±20% EV-demand variation. Two combined cases are also examined. The favorable condition uses load, PV, and EV scaling factors of 0.9, 1.2, and 0.8, respectively, whereas the stress condition uses 1.1, 0.8, and 1.2.

Across the nine operating conditions, the fixed nominal P–Q schedule retains feeder-loss reductions between 9.42% and 10.61% and VDI reductions between 16.48% and 19.37%. The relative mitigation therefore remains comparatively stable even though the absolute electrical stress of the feeder changes appreciably.

Load perturbation produces the clearest change in feeder severity. Increasing feeder loading by 10% raises the base daily loss to 5217.368 kWh/day and reduces the minimum voltage to 0.82422 p.u. Applying the unchanged coordinated schedule still reduces daily loss by 9.416% and raises the minimum voltage to 0.85325 p.u. Under the 10%-lower-load condition, the corresponding minimum voltage reaches 0.88025 p.u.

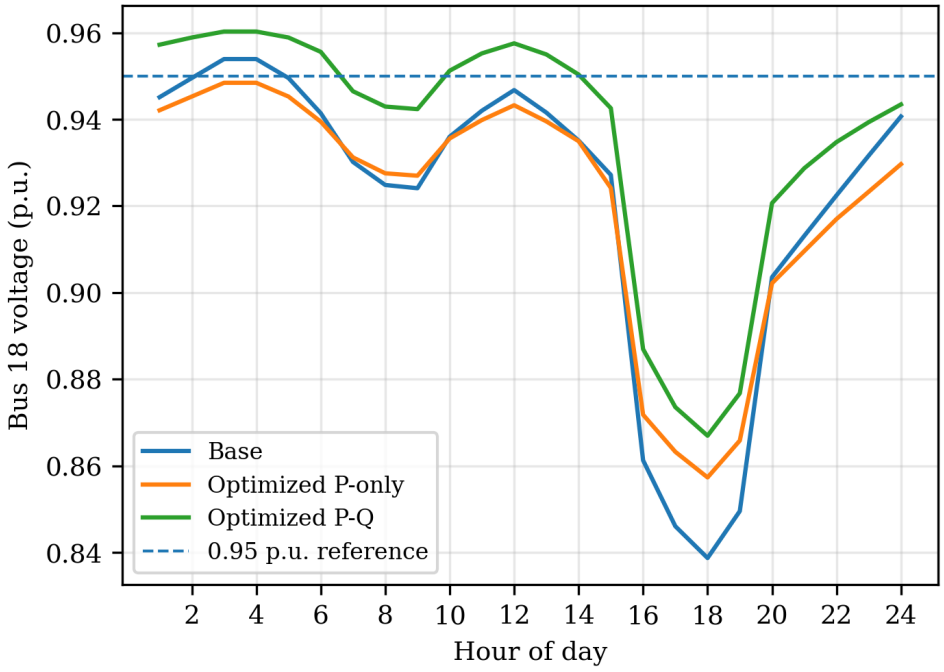


Fig. 8 Voltage magnitude at Bus 18 for the base, optimized P-only, and coordinated P–Q cases.

The PV perturbations have little influence on the worst minimum voltage. This follows directly from the temporal profiles: the critical voltage condition occurs during the evening EV-charging interval, when PV output has fallen to zero. PV variation therefore affects daytime branch currents and daily feeder losses but does not materially change the worst-voltage hour.

EV-demand variation has a stronger effect because it directly changes the electrical loading during the critical evening interval. A 20% increase in EV demand reduces the base minimum voltage to 0.82895 p.u., whereas a 20% reduction raises it to 0.84821 p.u. Coordinated P–Q operation improves both conditions but does not eliminate undervoltage.

Figure 13 emphasizes the distinction between persistence of the mitigation effect and voltage compliance. Across the perturbation cases, the coordinated schedule improves the minimum voltage by approximately 0.02693–0.02977 p.u. Under the combined stress condition, for example, the minimum voltage increases from 0.81414 to 0.84391 p.u. Although the improvement is technically meaningful, the resulting voltage remains well below 0.95 p.u. The robustness result therefore supports persistence of the mitigation effect, not guaranteed feeder-voltage compliance.

A local objective-weight check was also conducted for $w = 0.25$, 0.50, and 0.75 in Eq. (13). Using the nominal feasible P–Q solution as the warm start, all three tested values returned the same stored physical solution, corresponding to a daily

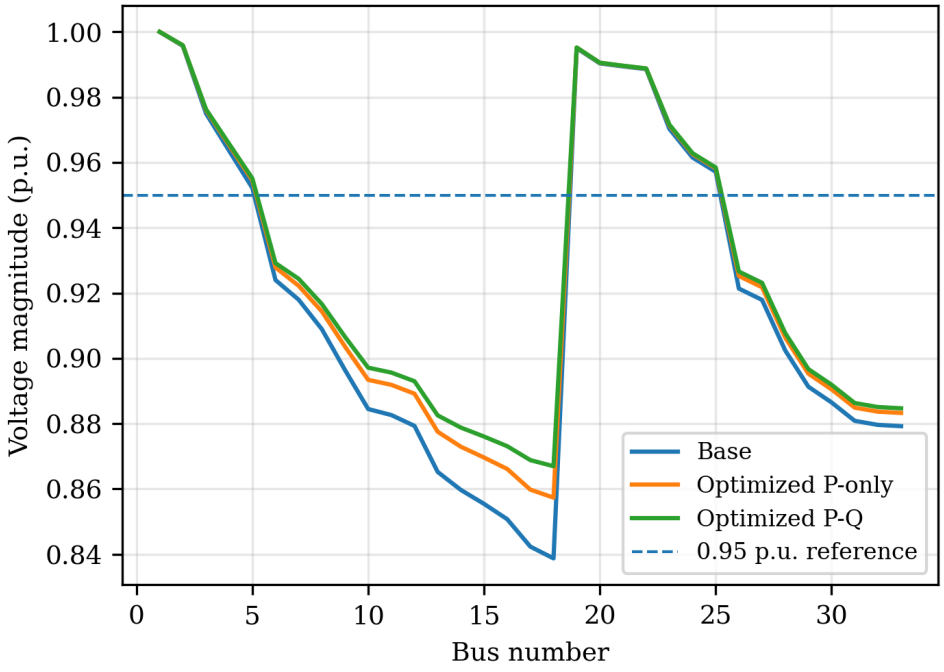


Fig. 9 All-bus voltage profile at the base-case worst operating hour (hour 18).

feeder loss of 3842.568 kWh/day, a daily VDI of 2.065514, a worst minimum voltage of 0.866951 p.u., and a minimum SOC of 19.410%.

This numerical invariance should be interpreted cautiously. It suggests that the active SOC limits and inverter apparent-power constraint strongly shape the local feasible region reached by the implemented solver. It does not establish uniqueness or global optimality, nor does it demonstrate that objective weighting is irrelevant over the complete feasible space. Because SLSQP solves a nonconvex constrained problem containing nonlinear power-flow calculations, the reported dispatch remains a locally optimized feasible solution.

5.4 Engineering Interpretation, Comparative Positioning, and Limitations

The principal engineering result is that the reactive-power capability of the smart inverter provides measurable network benefit beyond active-energy shifting alone. Under identical BESS hardware, P-only scheduling reduces daily feeder loss by 2.648%, whereas coordinated P–Q dispatch achieves a 9.965% reduction. The corresponding daily VDI reductions are 3.088% and 17.767%. Because storage capacity, inverter rating, feeder location, and external profiles are unchanged, the additional improvement can be associated with the availability and coordinated use of Q_{BESS}.

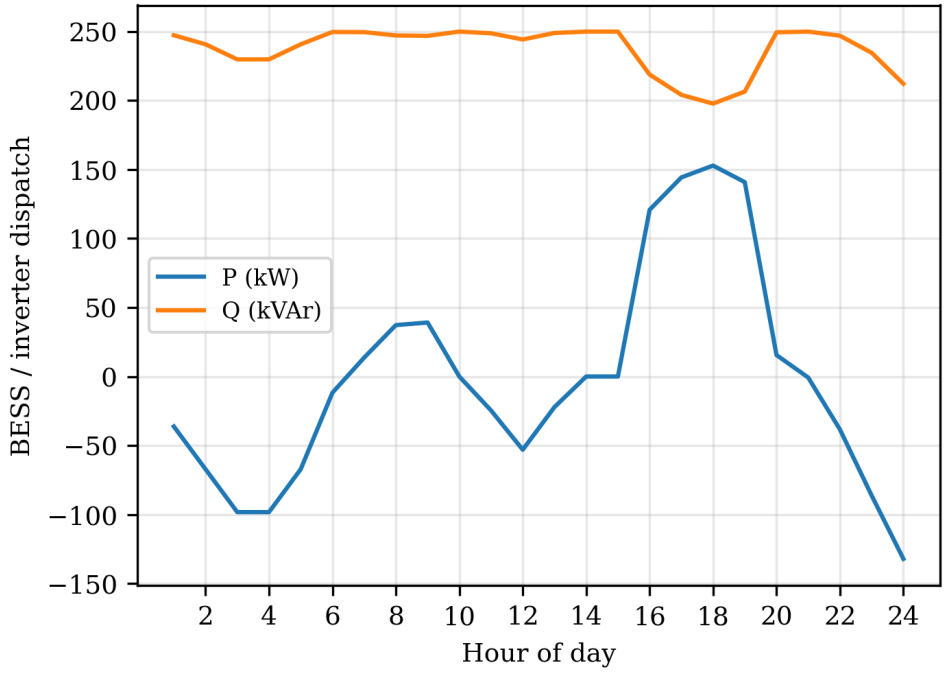


Fig. 10 Optimized active- and reactive-power dispatch of the 250-kVA smart inverter. Positive P denotes BESS discharge and positive Q denotes reactive-power injection.

This behavior is consistent with radial distribution-system physics. Active-power discharge reduces the real component of upstream branch loading, while reactive-power injection reduces the reactive component of branch current and supports local voltage. The combined reduction in current magnitude decreases resistive feeder losses and limits voltage drop along the electrically remote sections of the network. These trends are consistent with previous smart-inverter studies reporting voltage and loss benefits from inverter VAR control (Turitsyn et al. 2011; Demirok et al. 2011; Farivar et al. 2012).

The results also show why feeder-wide and local voltage metrics should be interpreted together. Coordinated P–Q control raises the worst minimum voltage from 0.83871 to 0.86695 p.u., while simultaneously reducing the daily VDI by 17.767%. The minimum voltage identifies the most severe single operating point, whereas VDI captures voltage displacement across all buses and hours. The relatively large VDI reduction therefore indicates that coordinated inverter control benefits a broader portion of the feeder even though the weakest operating point remains outside the 0.95-p.u. reference.

The residual undervoltage is an important engineering limitation rather than an unfavorable result to be omitted. A single 250-kVA inverter at Bus 18 cannot compensate indefinitely for feeder impedance and concentrated evening demand.

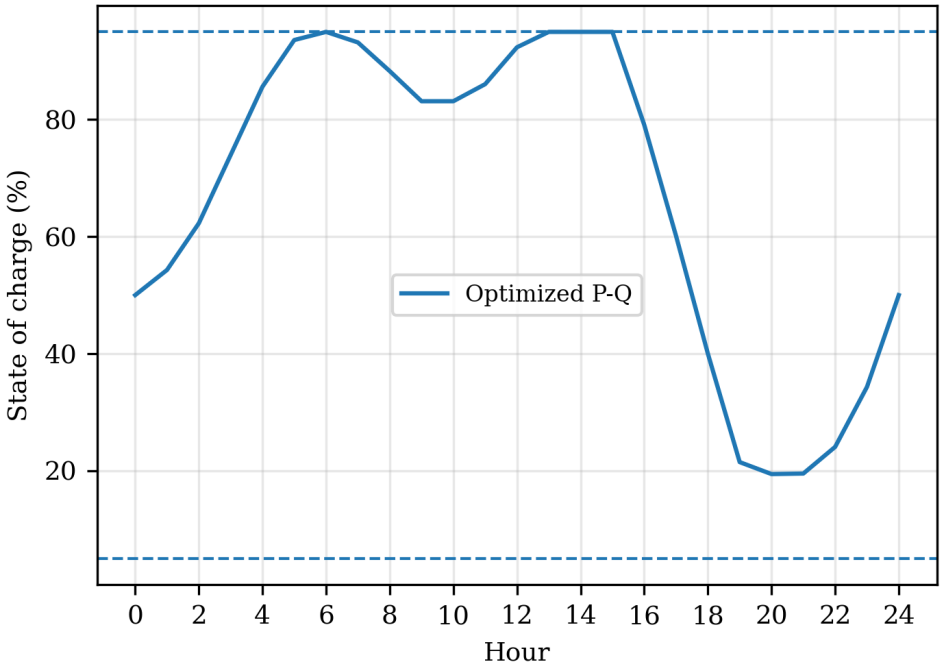


Fig. 11 SOC trajectory for the optimized P–Q case, including the specified 5% and 95% operating limits.

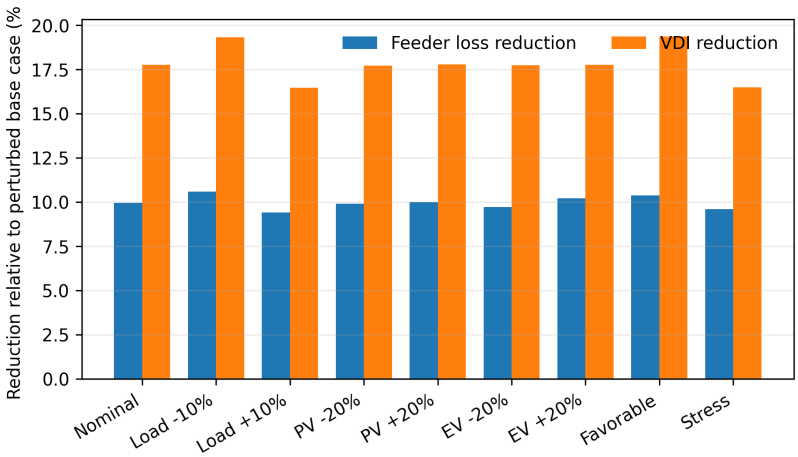


Fig. 12 Open-loop performance of the fixed nominal P–Q schedule under deterministic load, PV, and EV perturbations. Percentage reductions are calculated relative to the corresponding perturbed no-BESS base case, without scenario re-optimization.

The effectiveness of VAR control depends on available converter headroom, electrical distance from the substation, feeder impedance, and the coincident active-power

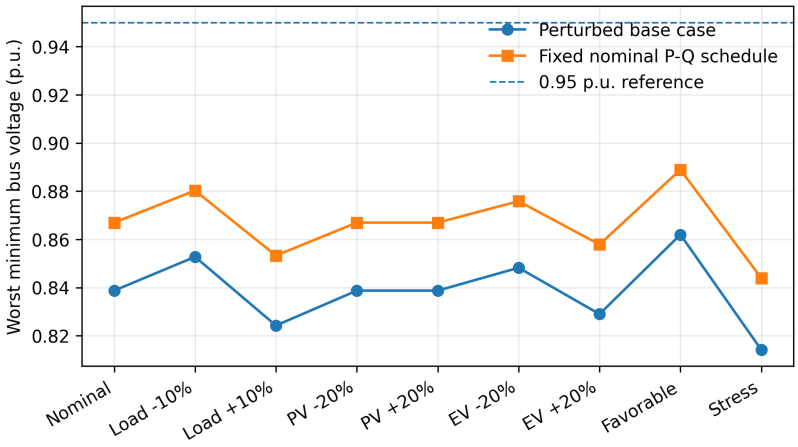


Fig. 13 Worst minimum bus voltage under the open-loop perturbation tests. The 0.95-p.u. line is retained as an engineering reference and is not reached under the more severe operating conditions.

requirement. This observation is consistent with previous investigations showing the importance of converter rating, location, and reactive-power margin (Demirok et al. 2011; Gush et al. 2021; Long and Kirschen 2022). Full voltage restoration under the studied stress condition would require additional network or converter resources, such as increased inverter kVA, multiple distributed VAR-capable devices, network reinforcement, or coordinated placement and sizing.

The increase in sub-0.95-p.u. bus-hours observed for the P-only case also demonstrates why BESS operation must be interpreted over the full time horizon. Although P-only dispatch raises the worst minimum voltage from 0.83871 to 0.85732 p.u., the number of low-voltage bus-hours increases from 338 to 355. Energy discharged at the evening peak must subsequently be recovered, and BESS charging shifts part of the feeder stress to other hours. Reactive-power support reduces this tradeoff because voltage can be influenced without directly changing stored battery energy.

The optimized converter trajectory additionally demonstrates that BESS energy capacity and inverter apparent-power rating play different roles. Increasing the battery energy capacity alone would not necessarily produce equivalent voltage support if the converter remains limited to 250 kVA. Conversely, sizing the inverter only for the maximum active-power requirement can leave insufficient reactive-power headroom during intervals requiring simultaneous active and reactive support. This distinction is relevant to practical BESS design because the converter kVA rating directly determines the feasible P–Q operating region.

Table 5 places these findings relative to representative smart-inverter, BESS, PV, and EV coordination studies. The purpose of the comparison is not to claim that the present formulation introduces a fundamentally new Volt/VAR concept or optimization algorithm. Rather, it identifies the methodological distinction of a controlled, fixed-hardware P-only/P–Q comparison with terminal-SOC neutrality and an open-loop profile-perturbation assessment.

The comparison confirms that the contribution of the present work lies in experimental design of the numerical study rather than introduction of a new general-purpose optimizer. The P-only and P–Q cases retain identical physical hardware and external operating conditions, thereby isolating the incremental network contribution of reactive-power capability. Daily energy neutrality is enforced through the terminal-SOC equality, preventing net battery depletion from being interpreted as an operational improvement. EV charging is modeled as an external feeder stress rather than as an additional controllable VAR source, which permits the capability of the BESS inverter itself to be evaluated directly.

The open-loop perturbation analysis provides an additional distinction. Because the nominal P–Q schedule is not re-optimized under each perturbed scenario, the analysis tests whether the original dispatch retains its electrical mitigation effect when the actual load, PV, or EV profile differs from the nominal condition. The results indicate that the relative reductions in feeder loss and VDI persist over the tested deterministic range, although absolute voltage remains strongly dependent on feeder loading and EV demand.

Several limitations define the scope of these results. The load, PV, and EV profiles are deterministic; the perturbation study is not a probabilistic or chance-constrained analysis. BESS location, energy capacity, active-power rating, and inverter rating are prescribed rather than jointly optimized. The IEEE 33-bus feeder is represented as a balanced radial network, and the model does not include battery degradation, electricity-price signals, capital cost, detailed converter losses, or unbalanced phase operation. In addition, SLSQP provides a local constrained solution and no claim of certified global optimality is made.

Overall, coordinated P–Q dispatch extracts substantially greater network value from the fixed smart-inverter BESS than active-power scheduling alone, particularly in terms of feeder-wide voltage deviation and daily resistive losses. At the same time, the remaining undervoltage demonstrates an important practical boundary: dispatch optimization can improve utilization of available converter capability, but it cannot substitute for sufficient inverter capacity, appropriate placement, or network reinforcement. Future work should therefore consider coordinated BESS location and sizing, converter-kVA selection, stochastic operating profiles, battery-degradation costs, unbalanced feeder models, and coordinated operation of multiple smart-inverter resources.

6 Conclusion

This study developed a reproducible 24-hour framework for coordinated active- and reactive-power dispatch of a smart-inverter BESS in the IEEE 33-bus radial distribution system. A backward/forward-sweep power-flow solver was integrated with SLSQP-based constrained optimization to compare three operating conditions under identical feeder, PV, EV, and hardware assumptions: a no-BESS base case, optimized P-only dispatch, and coordinated P–Q dispatch. By holding the BESS energy capacity, active-power rating, inverter rating, installation bus, and external operating

profiles fixed, the comparison isolates the incremental network contribution of inverter reactive-power capability.

For the specified 800-kWh BESS with a ±200-kW active-power limit and a 250-kVA inverter connected at Bus 18, coordinated P–Q dispatch reduced daily feeder active-energy loss from 4267.862 to 3842.568 kWh/day, corresponding to a 9.965% reduction, compared with 2.648% for P-only operation. The coordinated strategy also reduced the daily voltage-deviation index by 17.767% and improved the worst minimum bus voltage from 0.83871 to 0.86695 p.u. The SOC remained within the prescribed operating limits and returned to its initial value of 50%, confirming that the reported daily benefit was obtained through coordinated temporal power redistribution and inverter VAR support rather than net battery depletion.

The open-loop perturbation assessment showed that the fixed nominal P–Q schedule retained feeder-loss reductions of 9.42–10.61% and VDI reductions of 16.48–19.37% under the tested load, PV, EV, and combined profile variations without re-optimization. This indicates that the mitigation benefit is not confined to a single nominal operating trajectory. However, the absolute voltage response remains strongly dependent on feeder loading and EV demand, and the results should therefore be interpreted as persistence of the mitigation effect rather than guaranteed voltage compliance.

The remaining undervoltage also defines an important practical limitation. Although coordinated P–Q dispatch improves both feeder loss and voltage performance, a single 250-kVA inverter at Bus 18 is insufficient to restore all buses above the 0.95-p.u. reference under the selected severe operating condition. The results therefore emphasize that dispatch optimization can improve utilization of available inverter capability but cannot substitute for adequate converter rating, appropriate installation location, or network reinforcement. In addition, because SLSQP provides a locally optimized feasible solution, no claim of certified global optimality is made.

Future work should consider coordinated BESS placement and sizing, converter-kVA selection, multi-start or global optimization, stochastic load/PV/EV scheduling, battery-degradation and converter-loss models, unbalanced distribution feeders, and coordinated operation of multiple smart-inverter resources. These extensions would support progression from the present fixed-hardware performance study toward broader planning and operational applications for active distribution networks.

Statements and Declarations

Funding. This work was supported in part by the Institute of Vocational Education Eastern Region, Thailand.

Competing Interests. The authors declare that they have no competing interests.

Author Contributions. T.C. contributed to the conceptualization, methodology, software implementation, investigation, data analysis, and preparation of the original draft. S.N., P.P., S.S., and N.A. contributed to methodology development, technical validation, interpretation of the results, and critical revision of the manuscript. P.P. and T.K. contributed to supervision, technical review, and manuscript revision. All authors reviewed and approved the final manuscript.

Data Availability. The data generated and analyzed during the current study are available from the corresponding author upon reasonable request. The IEEE 33-bus test-system data used in the simulations are based on publicly available benchmark data, as cited in the manuscript.

Code Availability. The source code used to implement the backward/forward-sweep power-flow solver, the BESS dispatch optimization, and the numerical analyses is available from the corresponding author upon reasonable request.

Ethics Approval. Not applicable.

Consent to Participate. Not applicable.

Consent for Publication. Not applicable.

References

Ahlawat A, Das D (2023) Optimal sizing and scheduling of battery energy storage system with solar and wind DG under seasonal load variations considering uncertainties. J Energy Storage 74:109377. https://doi.org/10.1016/j.est.2023.109377

Babu KR, Khatod DK (2024) Smart inverter-based distributed Volt/Var control for voltage violation mitigation of unbalanced distribution networks. IEEE Trans Power Deliv 39:1481–1490. https://doi.org/10.1109/TPWRD.2024.3372603

Baran ME, Wu FF (1989) Network reconfiguration in distribution systems for loss reduction and load balancing. IEEE Trans Power Deliv 4:1401–1407. https://doi.org/10.1109/61.25627

Clement-Nyns K, Haesen E, Driesen J (2010) The impact of charging plug-in hybrid electric vehicles on a residential distribution grid. IEEE Trans Power Syst 25:371–380. https://doi.org/10.1109/TPWRS.2009.2036481

Dall'Anese E, Dhople SV, Giannakis GB (2014a) Optimal dispatch of photovoltaic inverters in residential distribution systems. IEEE Trans Sustain Energy 5:487–497. https://doi.org/10.1109/TSTE.2013.2292828

Dall'Anese E, Dhople SV, Johnson BB, Giannakis GB (2014b) Decentralized optimal dispatch of photovoltaic inverters in residential distribution systems. IEEE Trans Energy Convers 29:957–967. https://doi.org/10.1109/TEC.2014.2357997

Dall'Anese E, Dhople SV, Johnson BB, Giannakis GB (2015) Optimal dispatch of residential photovoltaic inverters under forecasting uncertainties. IEEE J Photovolt 5:350–359. https://doi.org/10.1109/JPHOTOV.2014.2364125

Das CK, Bass O, Kothapalli G, Mahmoud TS, Habibi D (2018) Overview of energy storage systems in distribution networks: placement, sizing, operation, and power quality. Renew Sustain Energy Rev 91:1205–1230. https://doi.org/10.1016/j.rser.2018.03.068

Demirok E, González PC, Frederiksen KHB, Sera D, Rodriguez P, Teodorescu R (2011) Local reactive power control methods for overvoltage prevention of distributed solar inverters in low-voltage grids. IEEE J Photovolt 1:174–182. https://doi.org/10.1109/JPHOTOV.2011.2174821

Eminoglu U, Hocaoglu MH (2009) Distribution systems forward/backward sweep-based power flow algorithms: a review and comparison study. Electr Power Compon Syst 37:91–110. https://doi.org/10.1080/15325000802322046

Farivar M, Neal R, Clarke C, Low S (2012) Optimal inverter VAR control in distribution systems with high PV penetration. In: IEEE Power and Energy Society General Meeting, pp 1–7. https://doi.org/10.1109/PESGM.2012.6345736

Gebbran D, Mhanna S, Chapman AC, Verbic G (2023) Multiperiod DER coordination using ADMM-based three-block distributed AC optimal power flow considering inverter Volt-Var control. IEEE Trans Smart Grid 14:2874–2889. https://doi.org/10.1109/TSG.2022.3227635

Ghazavi Dozein M, Gomis-Bellmunt O, Mancarella P (2021) Simultaneous provision of dynamic active and reactive power response from utility-scale battery energy storage systems in weak grids. IEEE Trans Power Syst 36:5548–5557. https://doi.org/10.1109/TPWRS.2021.3076218

Gush T, Kim C-H, Admasie S, Kim J-S, Song J-S (2021) Optimal smart inverter control for PV and BESS to improve PV hosting capacity of distribution networks using slime mould algorithm. IEEE Access 9:52164–52176. https://doi.org/10.1109/ACCESS.2021.3070155

Hu R, Wang W, Wu X, Chen Z, Jing L, Ma W, Zeng G (2022) Coordinated active and reactive power control for distribution networks with high penetrations of photovoltaic systems. Sol Energy 231:809–827. https://doi.org/10.1016/j.solener.2021.12.025

IEEE (2018) IEEE standard for interconnection and interoperability of distributed energy resources with associated electric power systems interfaces. IEEE Std 1547-2018. https://doi.org/10.1109/IEEESTD.2018.8332112

IEEE (2022a) IEEE guide for using IEEE Std 1547 for interconnection of energy storage distributed energy resources with electric power systems. IEEE Std 1547.9-2022. https://doi.org/10.1109/IEEESTD.2022.9849493

IEEE (2022b) IEEE guide for assessing, measuring, and verifying Volt-Var control and optimization on distribution systems. IEEE Std 1885-2022. https://doi.org/10.1109/IEEESTD.2022.9828004

Khajeh H, Parthasarathy C, Doroudchi E, Laaksonen H (2023) Optimized siting and sizing of distribution-network-connected battery energy storage system providing flexibility services for system operators. Energy 285:129490. https://doi.org/10.1016/j.energy.2023.129490

Kraft D (1988) A software package for sequential quadratic programming. DFVLR-FB 88-28, Institut für Dynamik der Flugsysteme, Oberpfaffenhofen, Germany

Long Y, Kirschen DS (2022) Bi-level Volt/VAR optimization in distribution networks with smart PV inverters. IEEE Trans Power Syst 37:3604–3613. https://doi.org/10.1109/TPWRS.2022.3142105

Mirafzal B, Adib A (2020) On grid-interactive smart inverters: features and advancements. IEEE Access 8:160526–160536. https://doi.org/10.1109/ACCESS.2020.3020965

Rahimi Far S, Moeini A, Chandra A, Kamwa I (2023) ADMM-based multi-objective control scheme for mitigating the impact of high penetration DER integration in the modern distribution systems. IEEE Access 11:38589–38603. https://doi.org/10.1109/ACCESS.2023.3266650

Richardson DB (2013) Electric vehicles and the electric grid: a review of modeling approaches, impacts, and renewable energy integration. Renew Sustain Energy Rev 19:247–254. https://doi.org/10.1016/j.rser.2012.11.042

Singhal A, Ajjarapu V, Fuller JC, Hansen J (2019) Real-time local Volt/VAR control under external disturbances with high PV penetration. IEEE Trans Smart Grid 10:3849–3859. https://doi.org/10.1109/TSG.2018.2840965

Soofi AF, Manshadi SD (2023) Unleashing grid services potential of electric vehicles for the Volt/VAR optimization problem. IEEE Trans Veh Technol 72:14115–14126. https://doi.org/10.1109/TVT.2023.3284757

Teng J-H (2003) A direct approach for distribution system load flow solutions. IEEE Trans Power Deliv 18:882–887. https://doi.org/10.1109/TPWRD.2003.813818

Turitsyn K, Šulc P, Backhaus S, Chertkov M (2011) Options for control of reactive power by distributed photovoltaic generators. Proc IEEE 99:1063–1073. https://doi.org/10.1109/JPROC.2011.2116750

Ustun TS, Hashimoto J, Otani K (2019) Impact of smart inverters on feeder hosting capacity of distribution networks. IEEE Access 7:163526–163536. https://doi.org/10.1109/ACCESS.2019.2952569

Virtanen P et al (2020) SciPy 1.0: fundamental algorithms for scientific computing in Python. Nat Methods 17:261–272. https://doi.org/10.1038/s41592-019-0686-2

Wong LA, Ramachandaramurthy VK, Taylor P, Ekanayake JB, Walker SL, Padmanaban S (2019) Review on the optimal placement, sizing and control of an energy storage system in the distribution network. J Energy Storage 21:489–504. https://doi.org/10.1016/j.est.2018.12.015

Wu R, Liu S (2023) Multi-objective optimization for distribution network reconfiguration with reactive power optimization of new energy and EVs. IEEE Access 11:10664–10674. https://doi.org/10.1109/ACCESS.2023.3241228

Yoshizawa S, Yanagiya Y, Ishii H, Hayashi Y, Matsuura T, Hamada H, Mori K (2021) Voltage-sensitivity-based Volt-VAR-Watt settings of smart inverters for mitigating voltage rise in distribution systems. IEEE Open Access J Power Energy 8:584–595. https://doi.org/10.1109/OAJPE.2021.3125013

Yuan Z, Wang W, Wang H, Yildizbasi A (2020) A new methodology for optimal location and sizing of battery energy storage system in distribution networks for loss reduction. J Energy Storage 29:101368. https://doi.org/10.1016/j.est.2020.101368

Zimmerman RD, Murillo-Sánchez CE, Thomas RJ (2011) MATPOWER: steady-state operations, planning, and analysis tools for power systems research and education. IEEE Trans Power Syst 26:12–19. https://doi.org/10.1109/TPWRS.2010.2051168

Table 1 Research Landscape and Positioning of the Present Study

Research stream	Representative studies	Typical resource/control	Primary focus	Position relative to this study
Radial distribution power flow	(Teng 2003; Eminoglu and Hocaoglu 2009)	Backward/forward-sweep and direct load-flow methods	Efficient nonlinear solution of radial feeders	Provides the numerical basis for the network solver but does not address coordinated BESS P–Q dispatch.
Smart-inverter Volt/VAR control	(Turitsyn et al. 2011; Demirok et al. 2011; Farivar et al. 2012; Dall'Anese et al. 2014a; Singhal et al. 2019)	PV and converter-interfaced DER reactive-power control	Voltage regulation, loss reduction, and coordinated Volt/VAR operation	Establishes the value of inverter VAR support, but generally does not isolate its incremental benefit through a fixed-hardware, energy-neutral P-only/P–Q comparison.
Multiperiod DER and BESS coordination	(Gebbran et al. 2023; Hu et al. 2022; Gush et al. 2021; Wong et al. 2019; Das et al. 2018)	BESS, PV, DER scheduling, sizing, and inverter control	Intertemporal coordination, hosting capacity, and storage operation	Introduces storage-energy coupling, although many studies address broader planning or multi-device coordination problems.
EV-related distribution operation	(Clement-Nyns et al. 2010; Richardson 2013; Soofi and Manshadi 2023; Wu and Liu 2023)	EV charging demand and converter-based reactive-power support	Charging impacts, voltage behavior, losses, and grid services	Motivates the EV loading scenario; in this study, EV charging is treated as an external feeder stress while the BESS inverter provides P–Q support.

Table 2 Principal Parameters of the 24-Hour Simulation and Optimization

Parameter	**Value**
Test feeder	IEEE 33-bus radial distribution system
Nominal feeder voltage	12.66 kV
System base	10 MVA
Simulation horizon	24 h
Time interval	1 h
PV connection	Bus 18
PV peak output	200 kW
EV charging connection	Bus 18
EV charging demand	400 kW, hours 16–19
EV power factor	0.95 lagging
BESS connection	Bus 18
BESS energy capacity	800 kWh
BESS active-power limit	$\pm$200 kW
Smart-inverter rating	250 kVA
Initial SOC	50%
Terminal SOC	50%
SOC operating range	5–95%
Charge/discharge efficiency	95% / 95%
Power-flow method	Backward/forward sweep
BFS convergence tolerance	10^{-9} p.u.
Maximum BFS iterations	100
Optimization method	SLSQP
Objective weighting	$w = 0.5$
Voltage reference	0.95 p.u. (reporting only)

Table 3 Computed Performance for the 24-Hour Operating Scenario

Case	Daily loss (kWh/day)	Loss reduction (%)	Daily VDI	VDI reduction (%)	Worst $V_{\min}$ (p.u.)	Bus-hours < 0.95 p.u.
Base: PV+EV, no BESS	4267.862	–	2.511772	–	0.83871	338
Optimized P-only	4154.861	2.648	2.434206	3.088	0.85732	355
Optimized P–Q	**3842.568**	**9.965**	**2.065514**	**17.767**	**0.86695**	**282**

Table 4 Open-Loop Performance of the Fixed Nominal P–Q Schedule Under Deterministic Profile Perturbations

Scenario	Base loss (kWh/day)	P–Q loss (kWh/day)	Loss red. (%)	VDI red. (%)	Base $V_{\min}$ (p.u.)	P–Q $V_{\min}$ (p.u.)
Nominal	4267.862	3842.568	9.965	17.767	0.83871	0.86695
Load −10%	3429.584	3065.767	10.608	19.322	0.85274	0.88025
Load +10%	5217.368	4726.119	9.416	16.481	0.82422	0.85325
PV −20%	4298.909	3872.770	9.913	17.731	0.83871	0.86695
PV +20%	4238.458	3813.960	10.015	17.800	0.83871	0.86695
EV −20%	4159.199	3754.995	9.718	17.751	0.84821	0.87582
EV +20%	4386.330	3938.322	10.214	17.782	0.82895	0.85787
Favorable combined	3308.714	2964.870	10.392	19.373	0.86197	0.88890
Stress combined	5386.660	4869.388	9.603	16.490	0.81414	0.84391

Table 5 Methodological Comparison With Representative Smart-Inverter, BESS, PV, and EV Coordination Studies

Study	System / resources	Optimization or control formulation	Energy / temporal coupling	EV modeled	Controlled P-only/P–Q comparison	Robustness / operating-variation assessment	Methodological distinction
Dall'Anese *et al.* (Dall'Anese et al. 2014a,b, 2015)	Residential PV inverters	Optimal active- and reactive-power inverter setpoints for feeder operation and voltage regulation	Not storage-energy coupled	No	No	Forecast uncertainty treated in subsequent work	Foundational optimal inverter dispatch; no BESS SOC or EV charging coupling.
Singhal *et al.* (Singhal et al. 2019)	High-PV distribution feeder	Adaptive local Volt/VAR control using smart PV inverters	Real-time control rather than daily storage scheduling	No	No	External disturbances explicitly considered	Focuses on adaptive local voltage control and stability rather than energy-constrained BESS dispatch.
Gush *et al.* (Gush et al. 2021)	PV and BESS on IEEE 33-node network	SMA-based optimization of smart-inverter Volt/VAR control, location, oversizing, and hosting capacity	Planning/control problem with BESS participation	No	No	Multiple operating/control cases	Broader planning and hosting-capacity scope; the present work isolates the incremental value of Q using fixed BESS hardware.
Hu *et al.* (Hu et al. 2022)	PV, BESS, OLTC, and capacitor banks on modified IEEE 33-bus system	Two-level coordination using MPC/MINP, modified NSGA-II, and leader–follower consensus	Yes	No	No	Operating variations considered within coordinated control	Uses several voltage-regulation resources; the present study deliberately uses a single fixed